Wear Mechanisms in Polyoxymethylene Spur Gears

S.M. Evans[a,b], P.S. Keogh[a]

[a] Department of Mechanical Engineering, University of Bath, Bath, BA2 7AY, UK

[b] Rotork plc, Brassmill Lane, Bath, BA1 3JQ, UK

ABSTRACT

The interaction of a polymer-steel spur gear pair is naturally prone to cause wear of the softer polymer material. Experimental equipment was therefore designed and constructed to run a polymer-steel spur gear pair with sufficiently accurate instrumentation such that the load and speed could be measured under a range of operating conditions. Plastic deformation features on the polymer teeth surface were observed through scanning electron microscopy and these are considered to be the primary sources of polymer gear wear during service. The wear mechanism is discussed and models are presented to describe the process by which it is created. This is due to the sliding/rolling under conforming contact conditions that are intrinsic to the involute spur gear pair. An iterative model based on the nonlinear properties of the polymer is presented, which shows how the material is deformed permanently and progressively under each load cycle. A second model also shows how the wear deformation features are created. Worn gear teeth were inspected and the quantity of material worn correlates well with the predicted wear volume.

Keywords: polymer gear wear; wear mechanism; polymer smear; polymer chain model

1 Introduction

Polymer gears are becoming widely used for general industrial applications and so it is increasingly important that their operating characteristics are understood in detail. Specifically, the details of wear mechanisms that result in material loss from the gears and the quantity of material lost should be considered. Walton and Shi [1] made observations of the different wear mechanisms of polymer gears. This work was built upon by the same research team in Breeds *et al*. [2], Walton and Shi [3] and Li [4] expand on this to include Scanning Electron Microscopy (SEM) inspection of worn gear teeth. In the study of material flow of PTFE made by Kar and Bahadur [5] the observation was also made that 'fibres' could be seen accumulating around the stylus of the profilometer used against the substrate material. A similar effect was observed in rubber and with both a stylus and a ball indenter by Briscoe [6], which gave flake like features which appear to be a function of bulk properties of the material. In the work of Kar and Bahadur and Tanaka *et al*. [7], images are presented of the surface of a PTFE sample that has been worn using a tribometer. The surface structures can be seen clearly and although some observations of the polymer 'fibres' grouping around the wearing stylus are possible, no further analysis is given. A question that Tanaka raises is whether a film is formed over the surface of the polymer due to the heating effect of the contact between it and the metal counterface.

Work by Kukureka *et al.* [8] describes a surface feature that has been formed into a flake, which could then be deformed such that pieces of the material are removed. This was then developed by Chen *et al.* [9] and is represented as macro-transverse cracks that propagate from the surface and which are then rolled into flakes as indicated in Kukureka's work. Xie and Williams [10] predicted the coefficient of friction and wear between a randomly rough hard surface and a softer surface. They used the statistical technique developed by Greenwood and Williamson [11] and expanded it to include specific plastic micro cutting of the softer material by the harder. This work was continued by Williams [12] to include the idea of plastic shakedown in the softer material, which is loaded beyond its elastic limit such that, as the load is released, permanent strain occurs in the material. If the load is cyclic then the permanent strain produces a ratchet effect in terms of deformation of the material. Bowden and Tabor [13] provide an extensive review of the literature to that date and they also conclude that atmospheric conditions (particularly relative humidity) are a factor in adhesion; this is confirmed by more recent work by Scholz [14].

Breeds *et al*. [2] identified that the driving and driven gears are moving in opposing directions and Kukureka *et al*. [15] present images of a wear mechanism between the gear teeth that is described as lateral cracking. However, these works were concerned predominantly with wear rates rather than specific wear mechanisms that are occurring at a microscopic level. Fisher *et al*. [16] found that surface roughness contributes greatly to the wear of a polymer in contact with a metal. The idea of surface roughness affecting the wear and efficiency of the sliding contact is corroborated by the work

of Xiao *et al*. [17]. Also, further validation of specific wear models for use in the medical prosthetics is to be found in Liu *et al.* [18]. Boissonnet *et al*. [19] found that wear particles get into the interface of the contact and act to increase the friction coefficient.

Chen *et al*. [9] used a simplified twin disc testing machine in which the relative slip speed between the two discs can be controlled to simulate the gear teeth action. They discovered that cracks propagated from the surface could be produced in the discs. Chen investigated further these cracks by sectioning the discs after testing. The twin disc test machine has the advantage over working on real gears that the worn surfaces are visible and easily accessed, however, the twin disc test machine has a deficiency as do all other gear-analogous test apparatus. In particular, the twin disc machine can be a combination of slip and roll, however, the slip and roll components of the contact action are in the same direction. A real gear pair in fact experiences roll and slip in opposing directions, so while the twin disc machine is a useful analogy to the real gear pair it can never accurately simulate the contact action.

Back to back testing with one electric motor back-driving another with the gear pair in between (the driven motor acts as a generator and so provides the load) was performed by Senthilvelan and Gnanamoorthy [20] and surface features were in fact observed that are relevant and interesting. However, no further analysis or conclusions for wear mechanisms are given. Hooke *et al*. [21] used a different type of machine for their investigations, a four-square rig. This machine uses a single electric motor to turn it but with two sets of spur gears connected across two parallel shafts, the driving set being case hardened steel gears. The other pair of gears to be tested were the polymer gears as performed by Mao *et al*. [22]. Measurement of the wear volume was performed by Wright and Kukureka [23], by use of a coordinate measurement machine (CMM) and the wear of various materials (all fibre reinforced) is plotted as function of the slip ratio of the gears as defined by their geometry. The results are thorough, but the data presented show a variation of around 70% in the wear volume measured, hence it would be difficult to draw any firm validation of a given model from these measurement data.

2 Background

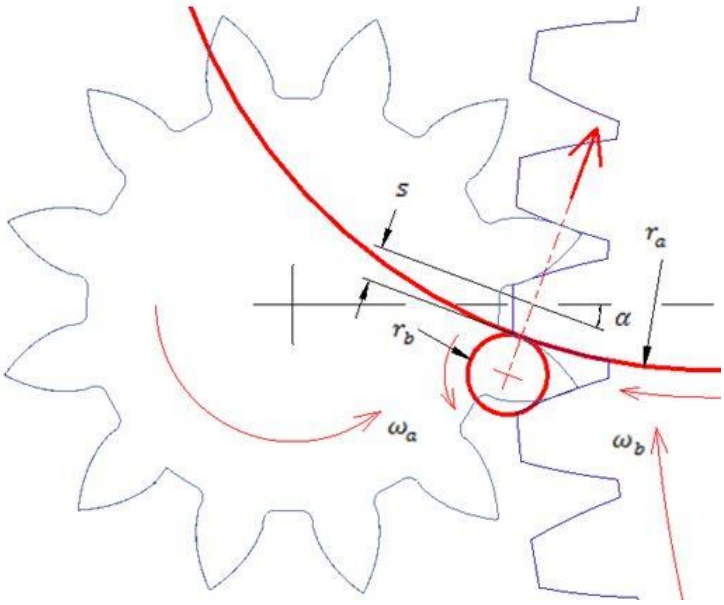

Fig. 1: Gear contact and the equivalent cylinders analogue

This paper identifies a specific and previously undocumented wear mechanism in Polyoxymethylene gears and provides a model that describes how material is removed. For a given load and speed, the volume of material that is removed by the mechanism is also predicted. The involute gear form is a gear tooth profile that allows constant and smooth power transmission from the driving gear (or pinion) to the driven gear. The involute profile is generated by sweeping an arc from the base circle of the gear to beyond the outer diameter of the gear, which produces the characteristic involute shape. This gear form is often described as being extremely efficient at transmitting power as it involves mainly a rolling contact between the teeth. This is true but sliding motion also exists between the teeth. This sliding motion gives rise to a particular contact mechanism between the teeth, and in the case of a steel pinion driving a polymer gear also produces distinct wear mechanisms. The instantaneous contact between the two gear teeth can be thought of as analogous to a pair of contacting equivalent cylinders whose diameters vary through the line of contact as described by Hamrock *et al.* [24]. The rotational speed of these equivalent cylinders varies through the line of contact (Figure 1) and so the slip speed can be calculated as the difference between their speeds is

$$v = \left(r_{bg} sin\alpha + s\right)\omega_b - \left(r_{ag} sin\alpha - s\right)\omega_a \quad (1)$$

where r_{ag} is the pinion pitch radius, r_{bg} is the gear pitch radius, α is the pressure angle (rad), s is the distance of the point of contact from the centre line, ω_a is the rotational speed (rad/s) of the pinion, and ω_b is the rotational speed (rad/s) of the gear. Accordingly, $r_a = r_{ag} sin\alpha - s$ and $r_b = r_{bg} sin\alpha +$

s. Figure 1 illustrates these parameters. From equation (1) it can be seen that the slip speed v will be positive until s becomes zero, at which point there will be no slip speed. The slip speed then becomes increasingly negative as the contact point moves away from the gear centre axis along the line of contact.

This paper identifies a wear mechanism through scanning electron microscopy images and provides a model to predict the quantity of material that is removed from the bulk of the gear by the mechanism during continuous operation of the gear pair under load. The wear mechanism identified by this research has been observed in Polyoxymethylene (POM - Delrin 100) gears that have been operated for approximately 10^6 cycles in an industrial product. The wear mechanism is replicated through bespoke experimental hardware.

3 Experimental Method

3.1 Experiment Hardware

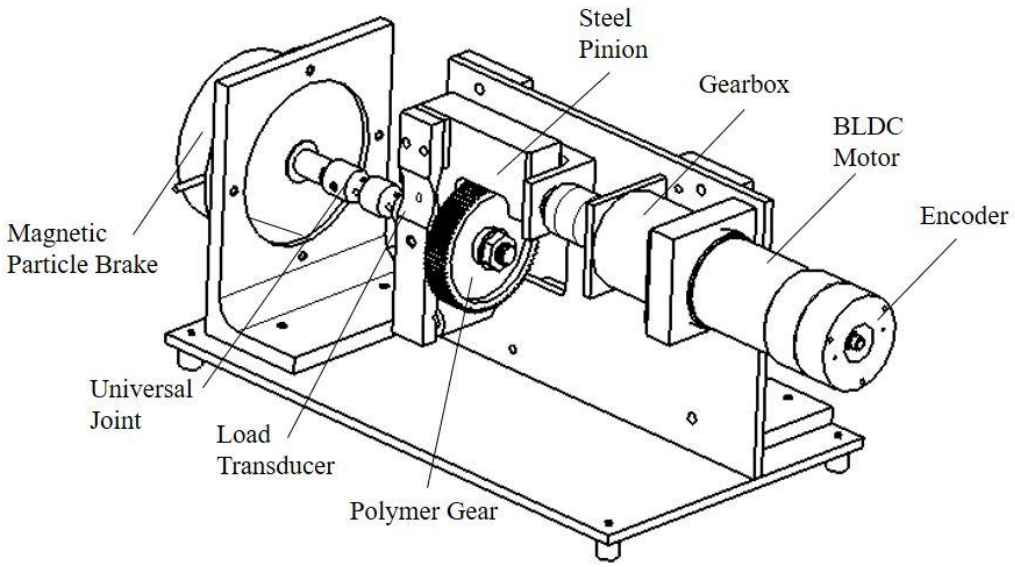

Fig. 2: Gear wear experiment hardware

Figure 2 shows the experimental system, which consists of a steel pinion running against a POM gear. The pinion is driven by a brushless DC electric motor and the POM gear reaction load is controlled by an electrically activated magnetic particle brake. The assembly is mounted in such a way that the reaction to loading is directed though a thin steel beam that is strain gauged and calibrated to measure the torque delivered through the POM gear to the magnetic particle brake. The speed of rotation is also measured accurately by way of an encoder mounted to the rear shaft of the motor. Using this equipment, it was possible to run the gears together for a known period of time at an accurately measurable torque and speed within 3% of the nominal maximum of each.

3.2 Sample Preparation

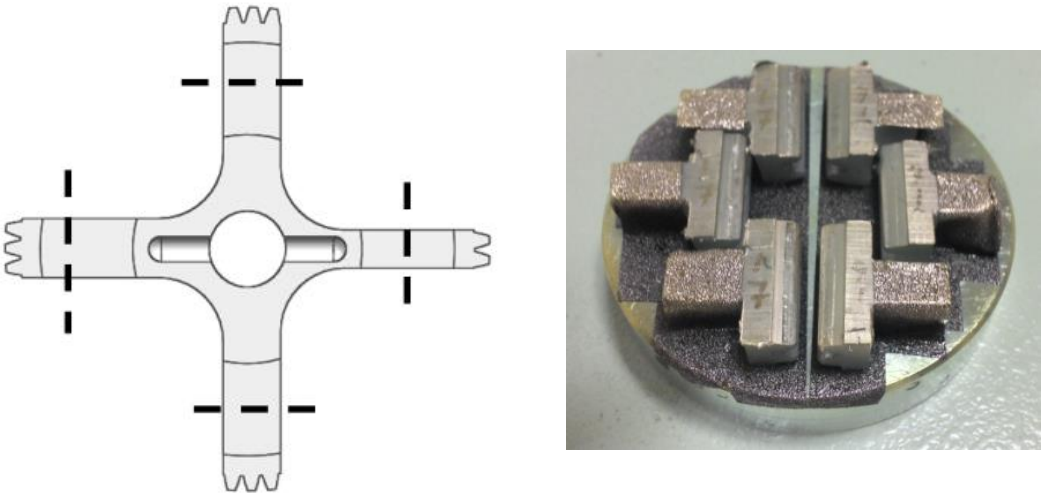

(a) (b)

Fig. 3: Gear sample preparation. (a) sample machining and (b) fully prepared sample stubs for SEM imaging

After running each sample at the specified load and speed, each gear was processed to extract four gear teeth samples. To prepare each test sample a procedure was developed to ensure that the tooth flanks of the samples were not disturbed or damaged and that a consitent methodology was followed. The following steps were undertaken:

- The gear was placed into a specially designed mandrel that held firmly the gear and could also be clamped in a milling machine
- The gear was then milled from 4 directions to expose 4 legs as shown in Figure 3a. Using a milling machine to do this ensured that each tooth flank could be exposed without risk of damaging its surface
- The legs were then cut at the dashed lines (Figure 3a) to leave samples to which two flank faces could be imaged easily
- The samples were fixed to aluminium stubs (Figure 3b) for mounting to the XYZ translation tables of a scanning electron microscope (SEM). They were fastened down with magnetic tape and additional tape was wrapped over the back of the sample to ensure electrical conductivity between the top face of the sample to the aluminium stub
- The samples were then placed for at least 24 hours in a vacuum chamber to decontaminate them for use in the SEM chamber
- They were then sputter coated with gold to ensure good conductivity with the SEM machine, which is necessary fo good quality imaging results

4 The Smear Mechanism

4.1 Observed Smear Mechanism

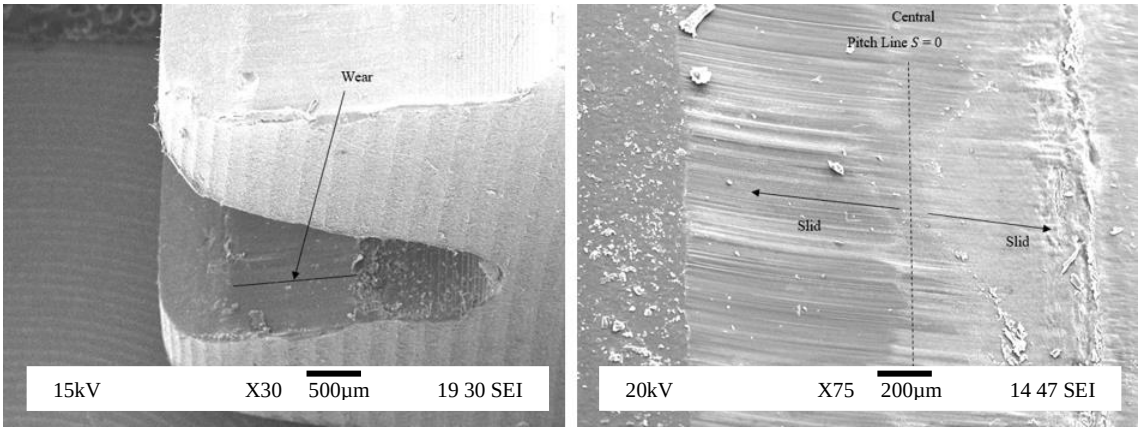

(a) (b)

Fig. 4: Worn teeth. (a) portion of teeth in profile and (b) plan view of worn area

Eleven gear pairs were run together using the experimental system an input torque of 0.85 Nm and a speed of 168 rpm. This speed and torque combination was used as it matches that of an industrial product manufactured by Rotork Controls. They were processed as described and the worn part of the gear flanks were inspected under the scanning electron microscope.

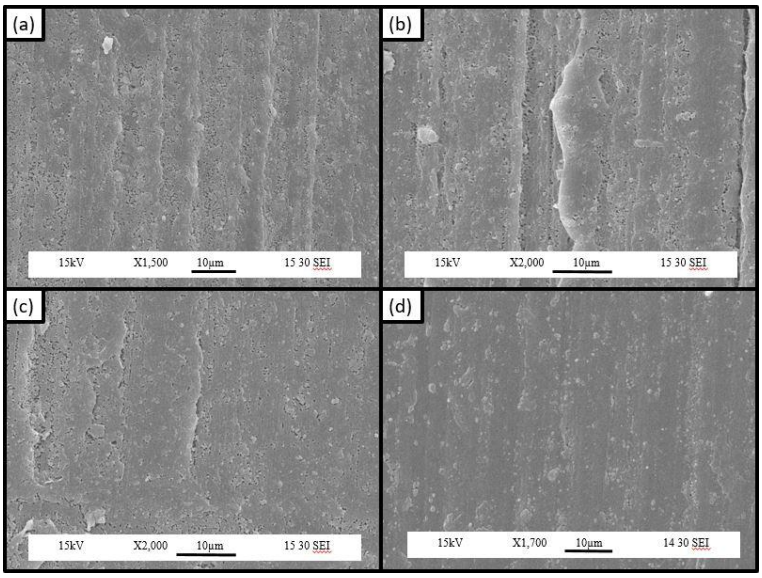

Fig. 5: Progression of sample wear. Sample numbers are shown for each sub-image for (a) – 0 cycles; (b) – 10 cycles; (c) – 100 cycles; (d) – 1000

Different elements of the worn areas of the gear tooth surface at increasing factors of magnification are now described. Figure 4a shows two worn teeth in profile, the area that has been in

contact with the steel pinion can be seen clearly. Figure 4b shows a plan view of the same tooth sample. The contact area is split top to bottom by a feature that has been generated by the position of the pitch line or where $s = 0$. Material can be seen to have been ejected from the contact area to the left of the area of contact. Figure 5 shows a series of samples that have undergone an increasing number of cycles of operation using the sample torque and speed input as specified. Sample (a) was an unused gear. Samples (b), (c) and (d) increased in operations from 10 to 100 to 1000 cycles, respectively. Machining marks can be seen on the teeth surface of the fresh sample, which were smoothed out as the gear was run up to 1,000 cycles.

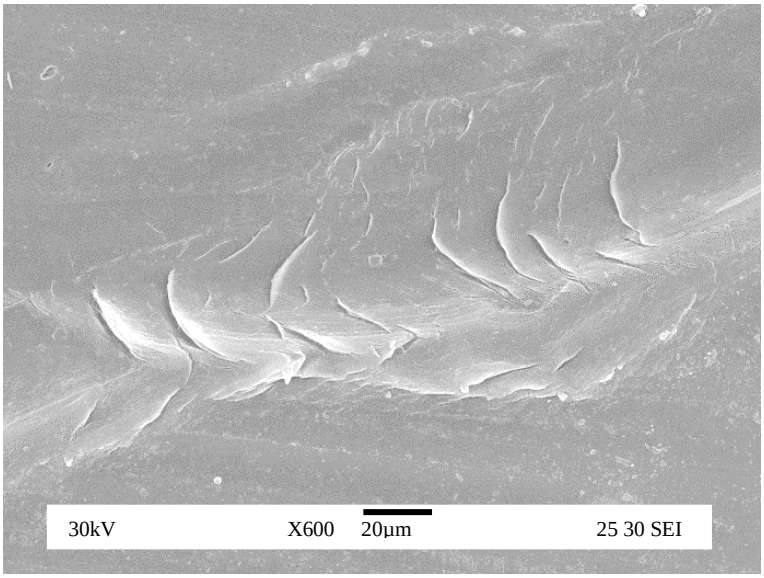

Fig. 6: Smearing of POM gear flanks after 6×10^6 cycles

Figure 6 shows a POM gear tooth flank that had been in continuous operation for approximately 6×10^6 cycles, then was processed and imaged using the SEM. The image is at 600 times magnification and is tilted at an angle of 40° to show the surface structures more clearly. The direction of slip is from the top right of the image to the bottom left. In the centre of the image several smear features are seen, which have been created by the contact conditions as the gears are driven together. They range in size and are approximately 10-40 µm in length and are in the order of 1-3 µm high. The swept forms of the features indicate that they are a function of the sliding contact between the gear teeth. The leading edge is thin and has been drawn up from the body of the material and on the lower part of the leading edge, small chain-like structures can be seen. Figure 7 shows a field of smears from a specimen; the image is at a magnification of 2700 and is tilted to better show the features. On this specimen the direction of slip-roll was from the right to the left. Fortuitously, the sample running has been stopped, prepared and imaged just at the point where material is breaking away from the leading edge of the smear. The debris can be seen to be forced in the direction of the sliding contact away from the smear feature. This debris is evident in used gearboxes as a fine nylon powder, with the newly identified wear mechanism being a contributor.

Figure 8 shows a smear feature field which was created by the experimental hardware shown in Figure 2. The direction of sliding is from the top right to the bottom left of the image. The features appear to be slightly less delicate than the features seen in Figure 6, but they are of similar size and

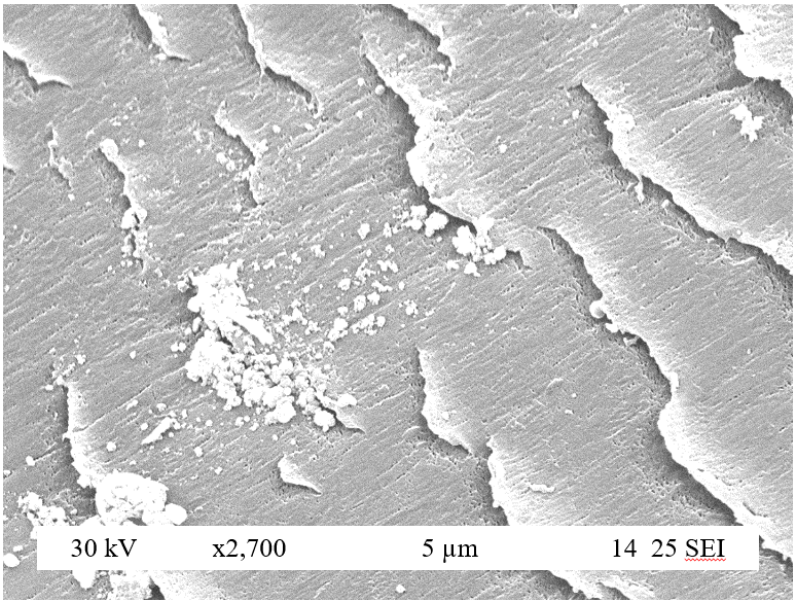

Fig. 7: Smear field showing debris breaking away from the leading edge

form. Additionally, debris can be seen breaking away from the trailing edge of the smear near the centre of the image and being dragged across the surface in the direction of the sliding action. It is proposed that this is the wear mechanism by which material is worn away from the surface of the gear. The smear is initiated and as the gear runs, this feature is then augmented by the action of the steel gear sliding and rolling over it, repeatedly. After many cycles the smear becomes elongated and more pronounced until it reaches the point where the material finally fails and breaks away from the

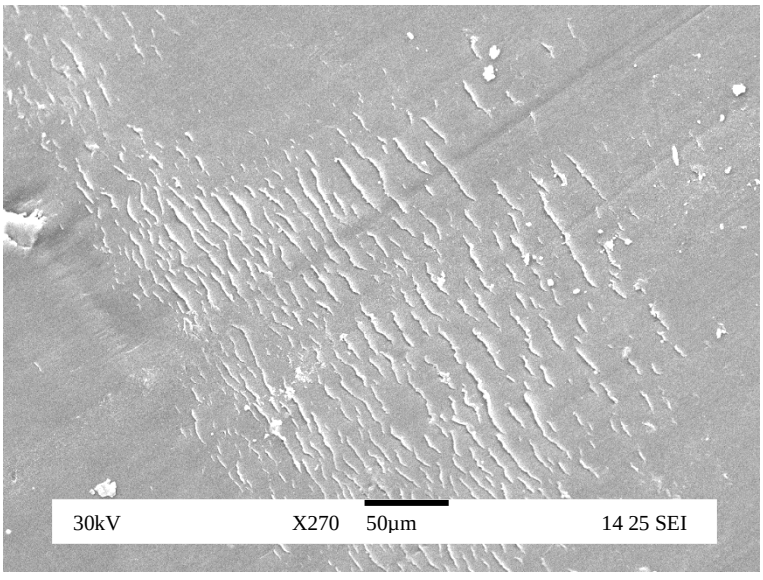

Fig. 8: Smears vary in pitch

leading edge of the smear, thus removing material. Figure 8 shows a field of smears; the sliding direction is from the top right of the image to the bottom left. The sliding across the surface due to slip speed is increasing from top right of the image to the bottom left. The pitch of the smears is increasing as the slip speed increases as further validation of the relationship between slip and smear creation.

4.2 Modelling the Smear Mechanism

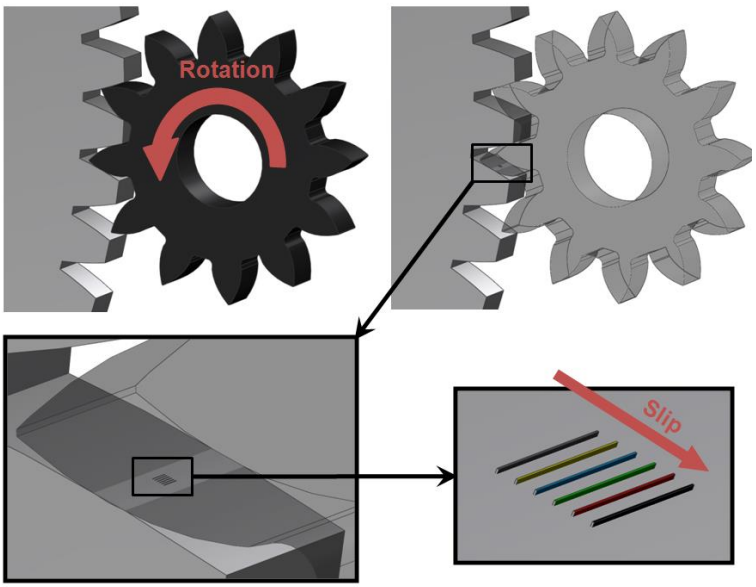

Fig. 9: Smear model representation

The characteristic of the contact mechanics between the gear teeth mean that the steel pinion is rolling in one direction over the polymer gear, but that the sliding between them is in the opposite direction. Therefore, if a group of polymer "chains" were subjected to this action over many cycles and that the strains levels were not sustainable, permanent deformation would occur. Figure 9 shows how rotation is translated into slip and shows a simplified and enlarged representation of a hypothetical group of six polymer "chains" underneath the contact between the steel pinion and the polymer gear. They will be stretched in the direction of the slip and because of the rolling action in the opposing direction will be subjected to a differing force from the rear chain to the front chain.

Contact Stress

The stress generated in the polymer can be evaluated from the force of the steel pinion pressing against the polymer gear flank due to torque transmission. In addition to the normal force directly due to torque, there will also be a tangential force. This tangential force is generated as a function of the normal force, the slip speed and the coefficient of friction between the steel and the polymer and is given by the standard friction representation,

$$F_T = \mu F_{norm} \tag{2}$$

As the material is loaded in this combination of normal and tangential forces a shear stress will be present. The stress components can be calculated as given using Johnson [25]:

$$\sigma_x = -\frac{2z}{\pi}\int_{-a}^{a}\frac{p(s)(x-s)^2 ds}{\{(x-s)^2+z^2\}^2} - \frac{2}{\pi}\int_{-a}^{a}\frac{q(s)(x-s)^3 ds}{\{(x-s)^2+z^2\}^2} \tag{3}$$

$$\sigma_z = -\frac{2z^3}{\pi}\int_{-a}^{a}\frac{p(s)ds}{\{(x-s)^2+z^2\}^2} - \frac{2z^2}{\pi}\int_{-a}^{a}\frac{q(s)(x-s)ds}{\{(x-s)^2+z^2\}^2} \tag{4}$$

$$\tau_{xz} = -\frac{2z^2}{\pi}\int_{-a}^{a}\frac{p(s)(x-s)ds}{\{(x-s)^2+z^2\}^2} - \frac{2z}{\pi}\int_{-a}^{a}\frac{q(s)(x-s)^2 ds}{\{(x-s)^2+z^2\}^2} \tag{5}$$

where $p(s)$ is the pressure distribution due to normal force, $q(s)$ is the shear stress distribution due to the frictional force, a is the half width of the pressure distribution, x is the horizontal dimension along the face of the gear flank surface, and z is the vertical dimension into the material. Note that the polymer gear flank is treated as an infinite half space. This approximation has been made as the radius of curvature of the polymer tooth flank is so much greater than that of the steel gear and it is also several orders of magnitude less stiff and so will conform to the shape of the steel pressing against it. The principal shear stress can then be found as

$$\tau_1 = \frac{1}{2}\{(\sigma_x-\sigma_z)^2 + 4{\tau_{xz}}^2\}^{1/2} \tag{6}$$

Under conformal contact with the steel pinion, the pressure distribution is

$$p(s) = p_o\left(1-\frac{x^2}{a^2}\right) \tag{7}$$

Also,

$$q(s) = \mu p(s) \tag{8}$$

Furthermore, $p_o$defines the stress in the material as a conformal contact between the steel and the polymer, thus

$$p_o = \frac{(1-v^2)}{(1-2v)}\frac{E}{(1-v^2)}\frac{a^3}{r\delta} \tag{9}$$

where v is Poisson's ratio for the polymer, E is its Young's modulus, r is the radius of curvature of the steel and δ is the depth of penetration of the steel into the polymer. These equations are then evaluated for a specific point along the line of contact, s = 1. Figure 10 shows the principal shear

stress in the polymer in a plane perpendicular to the axis of the gears local to the contact point, the x axis limits have been set equal to the half-width a (±0.16 mm). A maximum shear stress of 71 MPa is found located on the surface at the contact interface. A separate concentration of stress is observed beneath the surface consistent with that found in Hertzian contact theory. A layer of material

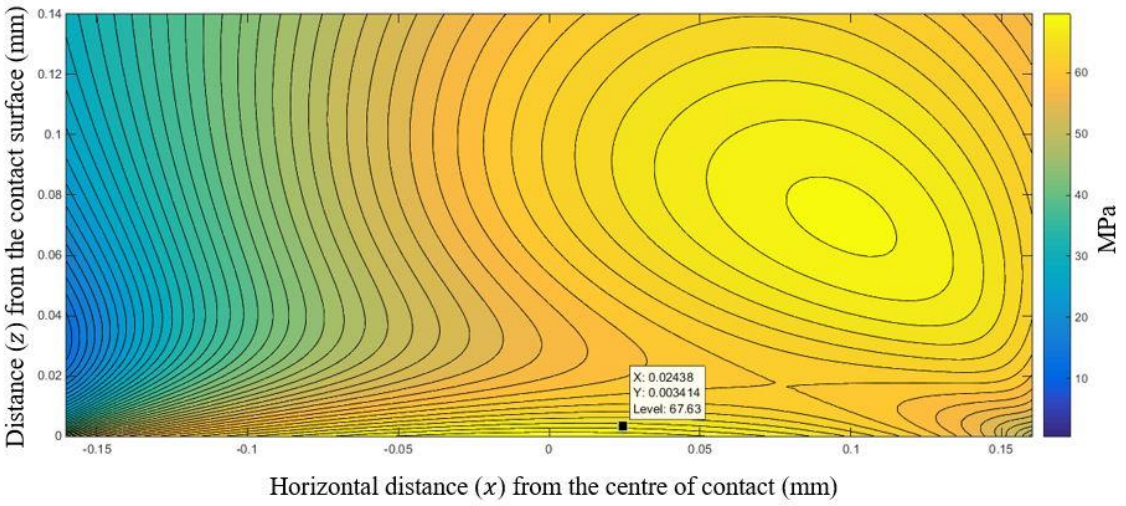

Fig. 10: Principal shear stress contours. Yield point of the slip layer – Conformal contact

approximately 3 μm in depth occurs for the length of the conformal contact, which is beyond the yield stress of the polymer (67 MPa).

For comparison, the Hertzian case is evaluated using the same method with

$$a = \left(\frac{3Pr}{4E}\right)^{1/3} \tag{10}$$

$$\delta = \frac{a^2}{r} \tag{11}$$

$$p_o = \left(\frac{6PE^2}{\pi^3 r^2}\right)^{1/3} \tag{12}$$

where P is the load per unit length. Figure 11 shows the principal shear stress in the polymer evaluated for Hertzian contact. The maximum stress is found to be 57 MPa, considerably lower than the conformal case and within the yield stress limit of the polymer material. The Hertzian contact induced principal shear stress distribution, the acute increase in stress at the edge of the contact being significantly different from the conformal contact case.

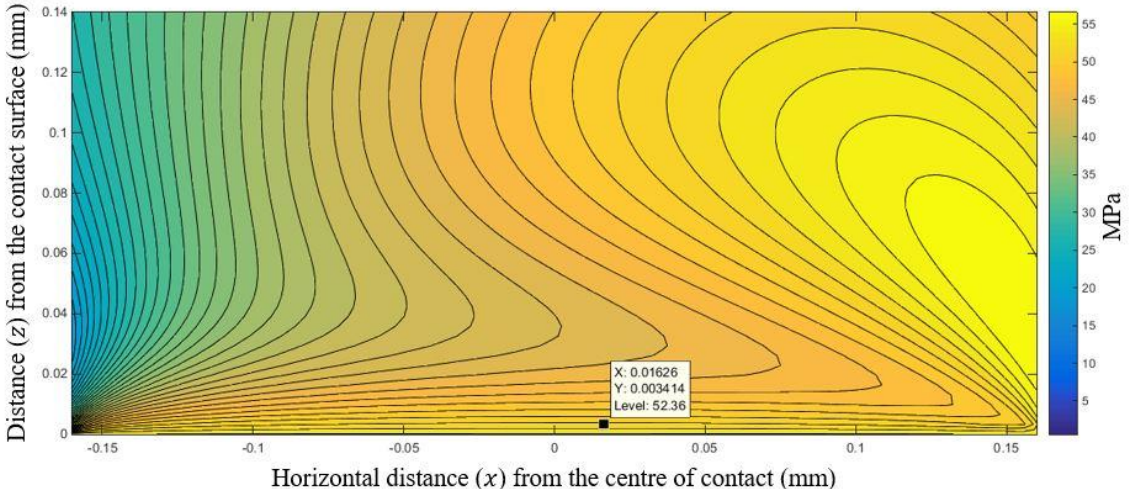

Fig. 11: Principal shear stress is below the polymer yield value under applied Hertzian contact stress

Slip Layer

Given that the polymer is predicted to yield around the contact zone to a depth of approximately 3 μm there will be a permanent deformation that persists after the gear tooth has passed. During each cycle of the gear this deformation will increase. Figure 12 illustrates the parameters for this where l is the slip layer depth, δ is the shear deflection due to strain in the polymer and F_T is the tangential force. The deflection is given as

$$\delta = \frac{\sigma}{E} l \tag{13}$$

and may be evaluated as 6.77×10^{-5} mm where F_T is 44.54 N. This figure is derived from the gear loading and geometry.

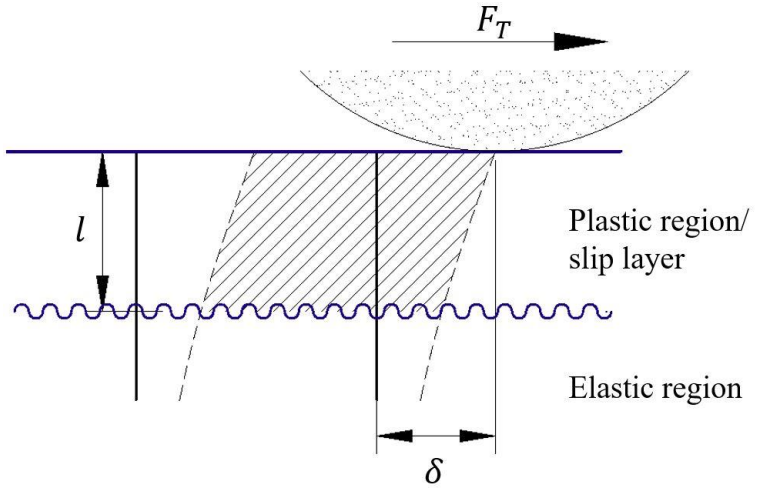

Fig. 12: Slip layer definition

This provides an evaluation of the strain in the material due to load. However, the power dissipated into the polymer material is a function of the slip velocity, which varies linearly with s through the contact zone and is zero when $s = 0$. As the contact zone processes across the tooth flank this variation in slip speed will cause the power dissipated to vary. It is proposed that this variation is the root cause for the formation of the smears. The slip speed decreases from left to right, which causes initially aligned polymer "chains" to undergo different levels of permanent deformation, the higher slip speeds on the left causing. Referring to Figure 8, a smear field has been created where smears have formed in lines and that they vary in pitch through the contact zone. The model presented in this section does not consider variations of the principal shear stress in the polymer across the width of the teeth. It is to be expected that small variations in contact conditions and material parameters will cause discontinuities is smear lines as evident in Figure 8. Given the general size of the smears, the model therefore predicts that smears will begin to form at around 300 cycles. Once initiated, they are drawn out until material breaks away from the leading edge as described in the following section.

Work Done

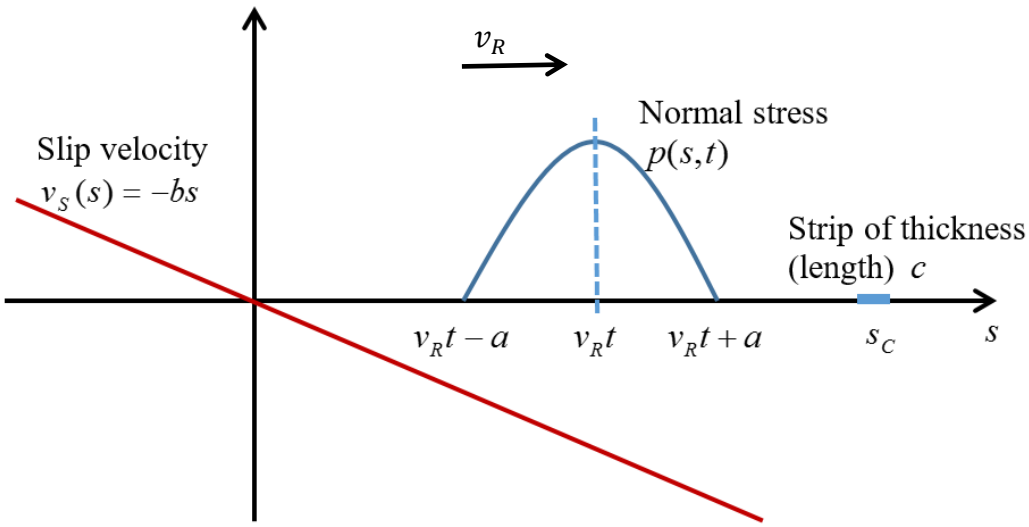

Fig. 13: Moving contact zone

Figure 13 shows the contact zone moving with a fixed velocity v_R due to rolling, with associated slip velocity $v_s(s)$ dependent on the position relative to the pitch point. The length of the contact zone, a, depends on the normal contact force. For cylinders in contact the normal stress is taken to be derived from the conformal case as given by equation (7):

$$p(s,t) = \begin{cases} p_o\left(1 - \left(\dfrac{s - v_R t}{a}\right)^2\right), & v_R t - a < s < v_R t + a \\ 0, & \text{elsewhere} \end{cases} \tag{14}$$

The normal force is

$$N = l \int_{v_R t-a}^{v_R t+a} p(s,t)ds = \frac{4}{3}\pi p_o l a \tag{15}$$

where l is the width of contact of the gear tooth flank. The area for consideration is a small stationary strip of length c under the contact and is relatively small in relation to that contact $2a$. The strip is the area considered to undergo smearing. The rolling velocity component v_R does not influence the slip velocity $v_s(s) = -bs$, which arises from the pinion/gear involute form. Here, $s = 0$ corresponds to the pitch point. Consider the stationary strip $(s_c - c/2 < s < s_c + c/2)$ on the gear surface (Figure 13), which is small compared to the length $(2a)$ of the contact zone. The strip is swept by the contact from $t = (s_c - a)/v_R$ to $t = (s_c + a)/v_R$. Over a time increment δt, the work done by the friction force at $s = s_c$ is, to first order quantities,

$$\delta W = \mu p(s_c, t) l c |v_s(s_c)| \delta t \tag{16}$$

Hence the work done at $s = s_c$ from $t = (s_c - a)/v_R$ to $t = (s_c + a)/v_R$ is

$$W = |v_s(s_c)| \mu l c \int_{(s-a)/v_R}^{(s+a)/v_R} p(s_c, t)dt = \mu P |v_s(s_c)| \frac{c}{v_R} \tag{17}$$

Setting $T_{cR} = c/v_R$ as the time to traverse a distance c at the rolling velocity v_R, the work done on the smear is

$$W = \mu P |v_s(s_c)| T_{cR} \tag{18}$$

This expression shows that the work done on the material is a function of the slip speed.

Permanent Deformation of the Surface

As the steel gear tooth contacts, the surface of the polymer is deformed to become conformal with the curvature of the steel pin. The stress generated at the surface is greater than the elastic limit of the polymer material, and in addition to this, the deformed polymer surface underneath the steel tooth becomes slightly extended than at rest. As the surface (to a depth of approximately 3 μm) is experiencing a stress beyond that which it can recover elastically and that the surface is stretched slightly beyond its original length, when the steel pin passes over, there remains an additional surface length. This creates a compressive stress in the surface of the polymer, whilst the underlying material is kept below its elastic stress limit. In this way, material is available to be moved by the slip action between the gear teeth by the work done on the surface as described equation (18). The characteristic of the deformations is seen to be in formations of smears or waves as illustrated in figures 6, 7 and 8.

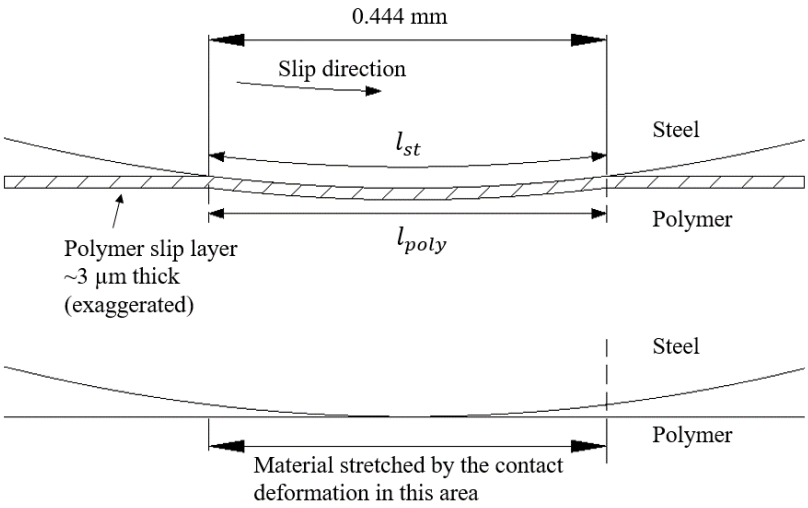

Fig. 14: Permanent deformation of the polymer surface due to loading by the steel

A 2-dimensional assessment may be made of the material moved by the teeth action based on the radii of the two contacting surfaces. The segment length of both the steel and polymer tooth is given by

$$l_{st} = r_{st} 2 \sin^{-1}\left(\frac{b}{2r_{st}}\right) \tag{19}$$

where b is the width of contact (shown as 0.444 mm in Figure 14), l_{st} is the segment length (for steel, in equation 19) and r_{st} is the radius, in this case steel. The total area therefore given by

$$A_{sme} = t_l\left(l_{poly} - l_{st}\right) \tag{20}$$

where A_{sme} is the area of material available to be smeared, l_{st} is the steel segment length, l_{poly} is the polymer segment length and t_l is the slip layer thickness. This model describes the action of a single

pass, or cycle, of the steel tooth over the nylon tooth. When the gearbox operates in service for many months or years, however, the teeth will undergo many millions of cycles. This action of deformation and release will therefore also repeat millions of times during the life of the gearbox. During this repetitive deformation and release cycling, smears will be formed and will grow until a fracturing failure at the leading edge of the smear will occur as seen in Figure 7.

5 Material Removed by the Smear Mechanism

5.1 Measurement of Material Wear Volume

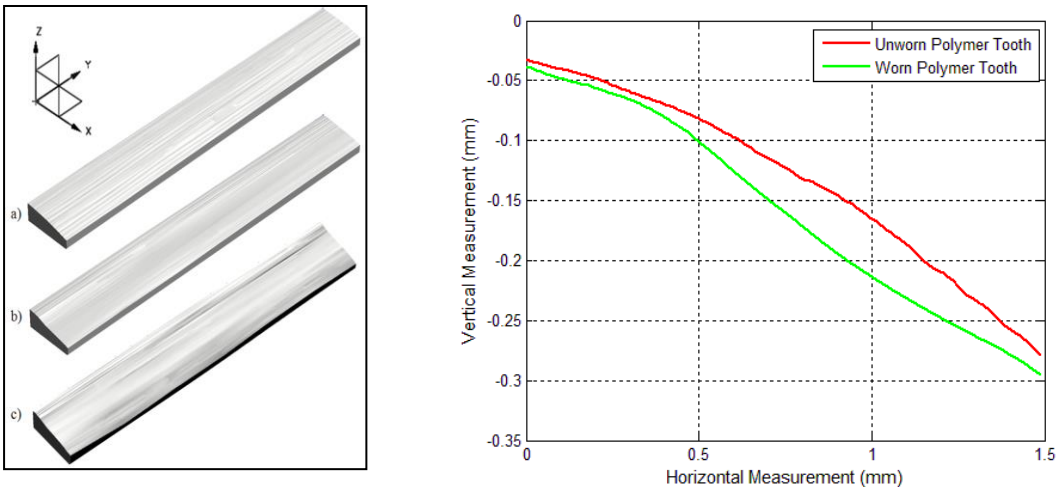

(a) (b)

Fig. 15: Measured gear teeth. (a) scanned gear teeth and (b) tooth profile measurement

The gear teeth were scanned to determine the shape and quantity of material that had been worn away during operation. The process of scanning was first to cut the gear tooth away from the gear wheel and then to use a profilometer to measure the tooth profile as a series of lines along the tooth from root to tip. Three gear teeth were scanned. The profile measurement was done along the *x*-axis as depicted in the coordinate system in Figure 14a. These profile data were then used to build Computer Aided Design (CAD) models from which the images in Figure 14a were generated. A series of profiles along the *y*-axis were generated at distances matching the measurement planes and were then swept together to form a solid model. Tooth a) is from an unused gear tooth, the surface of this scan shows clearly the machining marks from the manufacturing operation running in the *y*-axis direction. Its profile is consistent along the *y*-axis. Teeth b) and c) are scans of teeth that have been worn by 6×10^6 cycles of operation and the worn profiles can be seen as markedly different from the unused gear tooth in both surface roughness and gross form. Figure 14b shows one set of measurement data taken during the scanning process. A dip in the profile is seen beginning at $x = 0.4$ mm, which is where the steel tooth begins slipping in the positive x direction. The slip speed reduces to zero as the

contact point moves through the gear centre axis on the line of contact, which is at x = 1.1 mm. The slip then changes direction so slip in the negative x direction to the tip of the tooth at x = 1.6 mm.

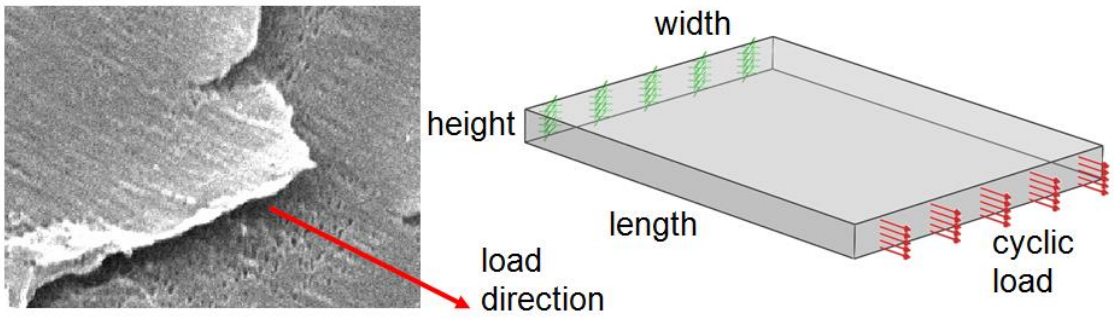

Fig. 16: Simplified smear block analogous to real smear

The CAD models allow the analysis of the surface of the gear teeth to measure the quantity of material removed by wear. This was done as a Boolean subtraction operation. An average of the worn teeth was taken in terms of volume and was then subtracted from the unworn tooth volume and multiplied by the number of gear teeth in the complete gear (75 in total). This gave the estimate of 77 mg of material worn away from the complete gear.

5.2 Predicting the Material Wear Volume

An individual smear can be modelled as a block of material with dimensions corresponding to the smear sizes observed through the scanning electron microscope images (Figure 15). If this analogous block were to be subject to a cyclic force of the same magnitude as the force applied due to the torque generated by the gear interaction, then it would be deformed. If the stress generated in the block exceeds its elastic limit, then the block would become permanently deformed before failure. A mathematical model has been developed that applies this scenario to a block of dimensions 20×40×3 μm (length×width×height) and iterates until failure occurs. The force is applied to the vertical face (width×height) of the smear as shown in Figure 15. The stress in the smear is given by

$$\sigma_p = \frac{F_p}{A_0} \tag{21}$$

where F_p is the pull force and A_0 is the initial face surface area of the smear (width×height). Figure 16 (upper plot) shows the stress/strain curve for POM as supplied by DuPont [26]. The strain is interpolated from this curve so that the remaining strain in the smear is found when the load is removed:

$$\epsilon_r = \epsilon_{int} - (\frac{\sigma_p}{\nabla}) \tag{22}$$

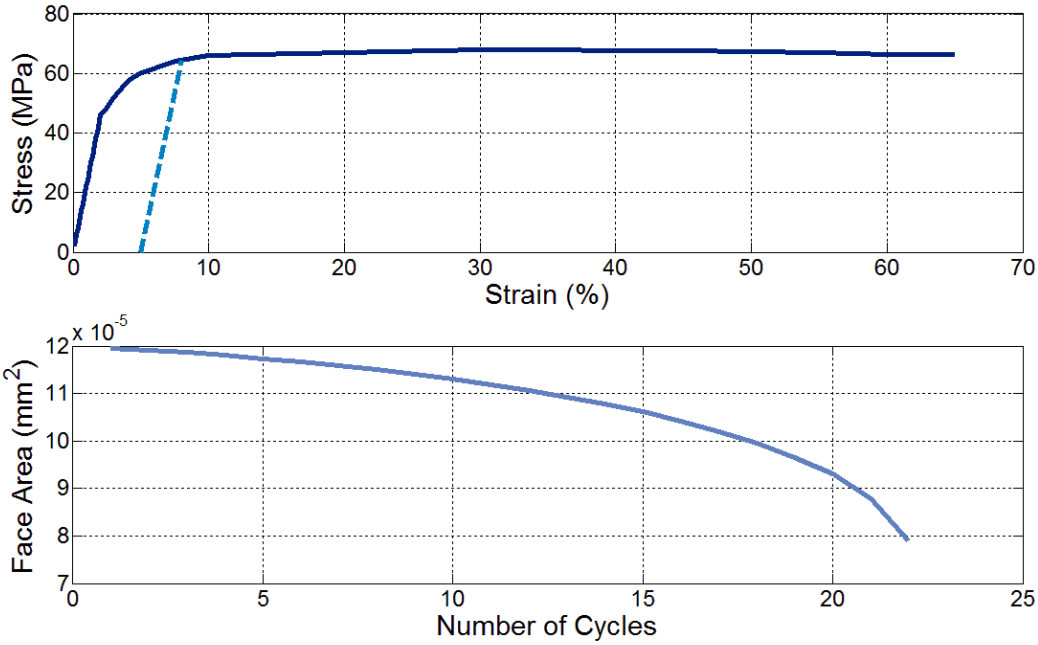

Fig. 17: Stress/strain and face area reduction

where ϵ_{int} is the strain interpolated from the stress/strain curve of the material and ∇ is the slope of the elastic part of the material curve. This calculation results in the dotted line in Figure 16 (upper plot) back to zero stress. Therefore, the new height and width of the smear can be calculated using the strain the material has undergone:

$$h_1 = h_0 - (2h_0 \nu \epsilon_r) \tag{23}$$

where h_0 is the initial height and ν is Poisson's ratio for the material (0.41, DuPont [26]). The width is calculated similarly and so the new face area of the smear is found. This step is repeated until an arbitrarily small value of the area is found at which point the iteration is stopped as it is assumed that the smear tip has fractured. The lower plot of Figure 16 shows the surface area of the face of the smear decreases as the stress cycles progress, until a definitive drop-off point is reached at around 22 cycles. This is the point at which the model assumes the smear must fracture. The size of the particle that has broken off from the smear is then evaluated as a percentage of the overall final smear cross-section and length.

There are a number of assumptions made in the model, namely the percentage area of material that is in contact and the percentage area that is a smear to be failed. Greenwood and Williamson [11] provide a substantial theoretical basis on the statistical quantity of asperities in contact at a surface interface and they find that this value is very low in comparison to the perceived area of contact in hard surfaces in elastic contact. However, they provide data to support the concept of a plasticity index, which has been interpolated to yield a plasticity index for this model. This provides the contact conditions variable. To address the question of the number of smears in the contact area, an

assessment was made from the SEM images to provide this. For 6×10^6 cycles, the model returns a total wear mass for the whole gear of 67 mg. This figure compares to 77 mg of material worn away from the gear as measured using the profile measurement technique discussed in Section 3.1.

6 Conclusions and Further Work

Experimental equipment was designed and constructed to operate a loaded pair of spur gears (where the gear was polymer and the pinion was steel) which was sufficiently well instrumented to accurately measure both the load and speed dynamically. The polymer gears were inspected using SEM techniques and a new mechanism of wear was identified, which is referred to as smears. Several different instances of the smear wear mechanisms are documented including an image capture of the moment at which worn material can be seen breaking from the leading edge of a smear, thereby confirming the mechanism by which material is worn away from the gear surface.

A phenomenological model is presented that describes how smears are initiated, formed and developed and is based on the slip/roll characteristics of the involute spur gear. Additionally, a model is presented that predicts the quantity of material removed by the wearing smear process. The mass of material removed from test gears during realistic operational conditions was also estimated from profile measurements and the modelled wear mass has shown to be of a similar order to that of the physical measurements taken. The measured mass of worn material value was 77 mg, while the modelled value was 67 mg. Further work would include a larger study of the frequency, distribution and size of the smears to establish a firm statistical basis for the model assumptions.

7 References

[1] D. Walton and W. Shi. A comparison of ratings for plastic gears. Proceedings of the IMechE, (1989), Volume 203, pp. 31 - 38.

[2] A.R. Breeds, S.N. Kukureka, K. Mao, D. Walton, C.J. Hooke, Wear behaviour of acetal gear pairs, Wear 166 (1993) 85-91.

[3] D. Walton and Y.W. Shi, Load sharing in metallic and non-metallic gears, Proceedings of the IMechE (1994) Volume 208, pp. 81 - 87.

[4] S. Li, Gear contact model and loaded tooth contact analysis of a three-dimensional, thin-rimmed gear, ASME - Journal of Mechanical Design (2002) Volume 124, pp. 511 - 517.

[5] M. K. Kar and S. Bahadur, Micromechanism of wear at polymer-metal sliding interface, Wear (1978) Volume 46, pp. 189-202.

[6] B. Briscoe. Wear of polymers: an essay on fundamental aspects. Tribolology International, (1981) Volume 14.4, pp. 231 - 243.

[7] K. Tanaka, Y. Uchiyama and S. Toyooka, The mechanism of wear of polytetrafluoroethelene, Wear (1973) Volume 23(2), pp. 153-172.

[8] S.N. Kukureka, Y.K. Chen, C.J. Hooke and P. Liao, The wear mechanisms of acetal in unlubricated rolling-sliding contact, Wear (1995), Volume 185, pp. 1-8.

[9] Y.K. Chen, S.N. Kukureka, C.J. Hooke and M. Rao, Surface topography and wear mechanisms in polyamide 66 and its composites, Journal of Materials Science (2000) Volume 35, pp. 1269-1281.

[10] Y. Xie, J.A. Williams, The prediction of friction and wear when a soft surface slides against a harder rough surface, Wear 196 (1996) 21-34.

[11] J.A. Greenwood, J.B.P. Williamson, Contact of nominally flat surfaces, Proceedings of the Royal Society of London A: Mathematical, Physical and Engineering Sciences 295 (1966) 300-319.

[12] J.A Williams,Wear modelling: analytical, computational and mapping: a continuum mechanics approach, Wear (1999) Volume 225, pp. 1-17.

[13] F.P. Bowden and D. Tabor, Friction, lubrication and wear: a survey of work during the last decade, British Journal of Applied Physics (1966) Volume 17, pp. 15 - 21.

[14] C.W.R. Scholz, Stick-slip and wear behaviour of ceramic and polymer materials under reciprocating sliding conditions. Turin (2013), World Tribology Congress.

[15] S.N. Kukureka, Y.K. Chen, C.J. Hooke and P. Liao, Surface failure mechanisms in polymer spur gears, Proceedings of the International Gearing Conference (1994), London. pp. 13-18.

[16] J. Fisher, D. Dowson, H. Hamdzah, H.L. Lee, The effect of sliding velocity on the friction and wear of UHMWPE for use in total artifical joints, Wear 175 (1994) 219-225.

[17] L. Xiao, S. Björklund and B.G. Rosén, The influence of surface roughness and the contact pressure distribution on friction in rolling/sliding contacts, Tribology International (2007) Volume 40, pp. 694-698.

[18] F. Liu, A. Galvin, Z. Jin and J. Fisher, A new formulation for the prediction of polyethylene wear in artificial hip joints, Proceedings of the IMechE Part H: Engineering in Medicine (2011) Volume 225.1 pp. 16-24.

[19] L. Boissonnet, B. Duffau and P. Montmitonnet, A wear particle-based model of friction in a polymer-metal high pressure contact, Wear (2012) Volume 286-287, pp. 55-65.

[20] S. Senthilvelan, R. Gnanamoorthy, Efficiency of injection moulded polymer composite spur gears, Proceedings of the IMechE Part J: Journal of Tribology 223 (2009) 925-928.

[21] C.J. Hooke, K. Mao, D. Walton, A.R. Breeds, S.N. Kukureka, Measurement and prediction of the surface temperature in polymer gears and its relationship to gear wear, ASME Journal of Tribology 115 (1992) 119-124.

[22] K. Mao, W. Li, C.J. Hooke, D. Walton, Polymer gear surface thermal wear and its performance prediction, Tribology International 43 (2010) 433-439.

[23] N.A. Wright and S.N. Kukureka, Wear testing and measurement techniques for polymer composite gears, Wear (2001) Volume 251, pp. 1567-1578.

[24] B.J. Hamrock, S.R. Schmid, B.O. Jacobson, Fundamentals of Fluid Film Lubrication (2nd edition, 2004), Marcel Dekker.

[25] K.L. Johnson, 1987. Contact mechanics. Cambridge University Press.

[26] Delrin®. www2.dupont.com. [Online].; 2014 [cited 2014 April 14. Available from: http://plastics.dupont.com/plastics/pdflit/americas/delrin/230323c.pdf.